

Wide binary companions to massive stars and their use in constraining natal kicks

Andrei P. Igoshev,¹^{*} Hagai B. Perets,¹

¹*Physics Department, Technion - Israel Institute of Technology, Haifa 3200002, Israel*

Accepted XXX. Received YYY; in original form ZZZ

ABSTRACT

The origin of ultra-wide massive binaries (orbital separations $10^3 - 2 \times 10^5$ AU) and their properties are not well characterized nor understood. Here we use the second Gaia data release to search for wide astrometric companions to Galactic O-B5 stars which share similar parallax and proper motion with the primaries. Using the data we characterize the frequency and properties of such binaries. We find an ultra-wide multiplicity fraction of 4.4 ± 0.5 per cent, to our completeness limit (up to ≈ 17 mag; down to G-stars at distances of 0.3-2 kpc, excluding stars in clusters). The secondary mass-function is generally consistent with a Kroupa initial stellar function; if extrapolated to lower mass companion stars we then might expect a wide-binary fraction of $\sim 27 \pm 5\%$. In addition we use these data as a verification sample to test the existence of ultra-wide binaries among neutron stars (NSs) and black holes (BHs). We propose that the discovery of such binary can provide unique constraints on the weakest natal kicks possible for NSs/BHs. If a compact object is formed in an ultra-wide binary and receives a very-low natal kick, such a binary should survive as a common proper motion pair. We therefore use Gaia data to search for ultra-wide companions to pulsars (normal and millisecond ones) and X-ray binaries. We find no reliable pairs. Future data could potentially provide stringent constraints through this method.

Key words: X-rays: binaries – astrometry – supernovae: general – stars: neutron – stars: black holes

1 INTRODUCTION

High-mass binaries have been extensively studied both observationally and theoretically (Sana et al. 2012; Duchêne & Kraus 2013; Moe & Di Stefano 2017). Close binaries play a critical role as the progenitors of type Ib/Ic supernovae and compact binaries, including X-ray binaries and gravitational-wave (GW) sources. Ultra-wide binaries ($> 10^3$ AU), however, received less attention.

Most stars are thought to form in stellar associations and clusters. In such dense environments ultra-wide binaries are "soft" (Heggie 1975). Even if they form in such environments, they are likely to be dynamically destroyed on short time-scales through binary-single and binary-binary interactions. The origins of wide binaries are therefore not well understood. Such soft binaries were suggested to be continuously destroyed and reform through dynamical captures, and those existing during the final stages and evaporation of the birth cluster/association, can then survive after the association/cluster dispersal (Kouwenhoven et al. 2010; Moeckel & Bate 2010; Moeckel & Clarke 2011) and give rise to observed

field wide-binaries. In principal, wide binaries could later be destroyed due to flybys in the field, however, these processes are typically not important for most of the relatively young objects studied here (see Appendix A for a brief discussion of this issue).

Although ultra-wide low-mass binaries have been explored and characterized (Duquennoy & Mayor 1991; Raghavan et al. 2010), their correspondent massive ultra-wide binaries, and in particular Galactic ones have been little explored. Here we use the new information from the second Gaia data release to identify and characterize Galactic massive (O-B5) main-sequence ultra-wide binaries ($10^3 - 2 \times 10^5$ AU separations). In this article we use the definition of wide binary following Andrews et al. (2017) and assume that two (or more) stars form wide binary if their properties are consistent with being gravitationally bound to each other on timescales comparable to the lifetime of the primary star.

Since massive stars are the progenitors of neutron stars (NSs) and black-holes (BHs), we also search for ultra-wide binaries among such compact objects, including ultra-wide companions to pulsars and millisecond pulsars (MSPs) and X-ray binaries (both high-mass and low-mass binaries). Since mass loss and NS/BH natal kicks affect the evolu-

* E-mail: ignotur@gmail.com

tion of such objects, ultra-wide binaries are not likely to be found among them. Nevertheless, as we discuss below, any discovery of ultra-wide bound companions to such objects could provide unique constraints on the existence and distribution of very low (or even zero) velocity natal kicks. We therefore provide a brief background on these issues before discussing our methods and results.

The article is structured as following: we begin with the description of formation of compact objects and compact binaries (Section 2), further we describe our method (Section 3) to identify ultra-wide pairs. We then describe our sample selection and our analysis of the samples of O/B stars (Section 4), pulsars (Section 5.1) and X-ray binaries (Section 5.2).

2 ULTRA-WIDE BH AND NS SYSTEMS AS PROBES FOR THE WEAKEST NATAL KICKS

A compact object (NS or BH) is born in a supernova explosion. The observed high velocities of NSs and some BH-binaries compared with the lower velocities typically observed for their progenitor OB massive stars suggest that both NSs and BHs are kicked at the moment of the explosion or immediately after. The origin of this velocity kick is still under debate (Lai 2001). The inferred NS natal kicks velocities range from possibly zero km s^{-1} to $\approx 1000 \text{ km s}^{-1}$ with an average speed of 364 km s^{-1} (Verbunt et al. 2017; Lyne & Lorimer 1994), while only ~ 3 per cent of pulsars appear to be born with velocities smaller than 60 km s^{-1} . The distribution of stellar-mass BH natal kicks is not known. The individual natal kicks for stellar-mass BH are usually estimated indirectly based on spatial distribution of low-mass X-ray binaries and seem to reach $\sim 100 \text{ km s}^{-1}$ (Jonker & Nelemans 2004; Repetto et al. 2012, 2017).

Some of the possible formation channels for NSs include cases where little mass loss and weak (or even zero) natal kicks are involved such as the case of an accretion-induced collapse of a white dwarf (Nomoto & Kondo 1991) or an electron capture supernova explosion (Miyaji et al. 1980; Nomoto 1984, 1987). The formation mechanism for BH natal kicks is also not understood. Although in some scenarios both NS and BH kicks can arise from the same mechanism (e.g. in the gravitational tug-boat mechanism by Janka 2017, 2013), they might have very different origins and/or properties. The lowest possible value for a natal kick to BH or NS is not known. As a result, population synthesis studies need to make specific assumptions regarding the distribution, and in some of them it is assumed that the natal kick can be exactly zero for a significant fraction of the objects (see e.g. Giacobbo & Mapelli 2019 for a recent double NS population synthesis and Toonen et al. 2018 for the white dwarf-NS merger rates). This assumption has to be tested observationally.

An X-ray binary (XRB) contains a compact object: NS or BH and a secondary star (donor) which loses material. XRBs are usually classified as low-mass or high-mass X-ray binaries (LMXBs or HMXBs) if the secondary mass is below $2M_{\odot}$ or above $8M_{\odot}$, respectively. An NS accreting gas in a LMXB can be spun up to form a millisecond pulsar (MSP)

with a white dwarf companion at later stages of its evolution (Bhattacharya & van den Heuvel 1991; Tauris 2011).

If a fraction of all compact objects receive no natal kick and lose only a moderate amount of mass, a third/second component with a large orbital separation can survive the supernova explosion and continue orbiting the XRB, MSP or normal pulsar, respectively. In this work we focus on ultra-wide binaries with orbital separations of $10^3 - 2 \times 10^5 \text{ a.u.}$. The corresponding large orbital periods of 0.1-10 Myr therefore prevent the detection of such companions by the timing technique in the case of normal pulsars and MSPs. According to the ATNF database v. 1.59¹ (Manchester et al. 2005) the longest period binary discovered by the timing techniques has a period of 20-30 years (J2032+4127 Lyne et al. 2015), although some pulsars are known to have wider companions detected through a combination of different techniques. This is the case of PSR J1024-0719 which has an orbital period of more than 200 yrs according to Bassa et al. (2016) and is in range 2-20 kyr according to Kaplan et al. (2016).

Close triples, such as the PSR J0337+1715 discovered by Ransom et al. (2014) with an orbital period of third companion of ≈ 327 days do not probe the lowest natal kicks because the third component of the PSR J0337+1715 could have been left bound to the system even after a natal kick with magnitude of 400 km s^{-1} (Tauris & van den Heuvel 2014). The LMXB V* V1727 Cyg (known as 4U 2129+47) seems to have a third component with an orbital period of $> 175 \text{ d}$ (Garcia et al. 1989; Bothwell et al. 2008; Lin et al. 2009). In this case too small natal kicks are not restricted (see Portegies Zwart et al. (2011) for a discussion of possible channels for the formation of MSP J1903+0327 through triple stellar evolution).

It might happen in rare cases that the magnitude and orientation of a strong natal kick is such that it allows for the formation of extremely eccentric wide binary with a large semi-major axis. However, our binary population synthesis models (see Appendix F) show that the probability for a chance formation of wide-binaries post-natal-kick is very low, $\approx 10^{-4}$ cases. Our small sample size of ≈ 50 NSs, therefore makes it unlikely to find kick-formed wide-binaries.

We propose to use ultra-wide binaries to probe the weakest natal kicks (a few km s^{-1} or even a fraction of km s^{-1}) by searching for wide astrometric pairs with common parallax and proper motion where one of the components is XRB, MSP or normal radio pulsar. This study follows to some extent the idea by El-Badry & Rix (2018) to probe the possible natal kick velocity of white-dwarfs. In order to identify wide pairs with NS/BH compact objects components we use the Gaia second data release following the same principles we use for the study of wide companions to massive OB stars. These methods are described in the following.

3 METHODS

For each of our objects (O/B star, HMXB, LMXB, pulsar or MSP) we select from the Gaia database all the stars found

¹ <http://www.atnf.csiro.au/research/pulsar/psrcat>

at angular distance up to

$$\theta_{\max} [\text{arcsec}] = 2 \times 10^2 \varpi [\text{mas}] \quad (1)$$

from our primary target. This choice is motivated by a fact that the number of chance aligned stars grows fast at distances $> 2 \times 10^5$ a.u. We keep only stars with measured parallax and proper motion with relative errors which are less than a third of their value. We also check the quality of the five-parameters astrometric solutions for which we used a criterion similar to [Lindgren et al. \(2018\)](#):

$$\sqrt{\frac{\chi^2}{\nu' - 5}} < 1.2 \max(1, \exp(-0.2[G - 19.5])) \quad (2)$$

where χ^2 is `astrometric_chi2_al` and ν' is `astrometric_n_good_obs_al` from the Gaia database.

For each pair we compute following values: angular separation at the sky $\Delta\theta$, difference in parallax $\Delta\varpi$ and its error $\sigma_{\Delta\varpi}$, difference in proper motion $\Delta\mu$ and its error $\sigma_{\Delta\mu}$ and the possible expected difference in proper motion due to orbital motion μ_{orb} . In these calculations we follow the technique described in [El-Badry & Rix \(2018\)](#). The angular distance at the sky is:

$$\Delta\theta = \sqrt{(\alpha_p - \alpha_*)^2 \cos^2 \delta_p + (\delta_p - \delta_*)^2} \quad (3)$$

where α_p , α_* , δ_p and δ_* are the right ascension and declination of the primary and its possible second/third component, respectively. The difference in parallax is:

$$\Delta\varpi = |\varpi_p - \varpi_*| \quad (4)$$

where ϖ_p and ϖ_* are the parallaxes of the primary and the distant candidate companion, respectively. The error of the parallax difference is:

$$\sigma_{\Delta\varpi} = \sqrt{\sigma_{\varpi,p}^2 + \sigma_{\varpi,*}^2} \quad (5)$$

The difference in proper motions is:

$$\Delta\mu = \sqrt{(\mu_{\alpha p} - \mu_{\alpha*})^2 + (\mu_{\delta p} - \mu_{\delta*})^2} \quad (6)$$

where the proper motion in the right ascension direction is μ_{α} and in declination is μ_{δ} . The error in the proper motion difference is:

$$\sigma_{\Delta\mu} = \frac{1}{\Delta\mu} \sqrt{(\sigma_{\mu_{\alpha p}}^2 + \sigma_{\mu_{\alpha*}}^2) \Delta\mu_{\alpha}^2 + (\sigma_{\mu_{\delta p}}^2 + \sigma_{\mu_{\delta*}}^2) \Delta\mu_{\delta}^2} \quad (7)$$

where $\sigma_{\mu_{\alpha p}}$ and $\sigma_{\mu_{\alpha*}}$ are errors of the proper motion in the right ascension direction for the primary and secondary stars. The possible expected difference in proper motion due to orbital motion is computed as:

$$\mu_{\text{orb}} \approx 0.53 \text{ mas year}^{-1} \left(\frac{\varpi_p}{\text{mas}} \right)^{3/2} \left(\frac{\Delta\theta}{\text{arcsec}} \right)^{-1/2} \quad (8)$$

The value is computed as maximum proper motion due to motion on circular orbit around a star with a mass $7M_{\odot}$:

We use the following conditions to identify the binaries:

- (i) $\Delta\varpi < 2\sigma_{\Delta\varpi}$
- (ii) $\Delta\mu < (\mu_{\text{orb}} + 2\sigma_{\Delta\mu})$
- (iii) $\sigma_{\Delta\varpi} < 0.12 \text{ mas}$
- (iv) $\Delta\mu < 3\mu_{\text{orb}}$
- (v) $\sigma_{\Delta\mu} < 0.16 \text{ mas year}^{-1}$

These conditions are implemented as an ADQL request, see [Appendix B](#). The first two conditions allow us to select stars which are close in phase-space. The last three conditions are set to remove a vast number of chance alignment of unassociated stars. These conditions were chosen using a displaced sample and visual inspection, as we describe in the following Section. The list of binaries with massive primary star identified by this method contains a significant number of members of open clusters. We describe the identification procedure for open clusters in the [Section 3.2](#).

3.1 Chance alignment considerations

The distribution of projected separations and the inferred binary fraction are affected by chance alignments of background stars. The main challenge in using this method is therefore to identify a boundary between a chance alignment identification and the identification of actual physical pairs.

First we visually inspect the sample using only $\Delta\theta$, $\Delta\mu$ and $\Delta\varpi$ following [Lépine & Bongiorno \(2007\)](#) to check if any binaries can be found in the sample. The distribution of these values for the O/B sample is shown in [Figure 1](#) (right panel). We then change the declination of each O/B star in our sample by adding $50'$ (taking into account large parallax of $\varpi = 16 \text{ mas}$ for some close massive stars) and plot the angular separations and the difference in the proper motion again, see [Figure 1](#) (left panel). A clear presence of stars in the left lower corner of the plot convinces us that the sample contains real binaries. At this point we choose a values of 0.12 mas as the critical value for the error in parallax difference ($\sigma_{\Delta\varpi}$), $0.16 \text{ mas year}^{-1}$ as the critical value for the error in the proper motion difference ($\sigma_{\Delta\mu}$) and the requirement that $\Delta\mu < 3\mu_{\text{orb}}$. The exact choice is somewhat arbitrary; and we decided on these values as to identify the binaries seen by eye in [Figure 1](#).

In order to estimate the chance alignment we run the complete search for binaries with chosen parameters for all massive stars, by first shifting their declination to $50'$ in positive direction and then shifting to a negative direction. We identified 0 chance aligned pair in both cases.

3.2 Cluster identification

Many massive stars belong to open clusters or form OB associations. In such associations each star could potentially have many identified false wide companions. To simplify the analysis we therefore consider only field stars and discard stars in stellar clusters/associations in our analysis.

In order to identify the field vs. cluster stars we make use of the open cluster catalogue by [Cantat-Gaudin et al. \(2018\)](#) who identified 1229 open clusters using the second Gaia data release. For each O/B star with identified wide pairs we find all the clusters in the same region of the sky up to 1 degree around this star. An O/B star is considered by us to be a member of a cluster if its parallax is within 0.3 mas from the cluster parallax and its proper motion is within 2 mas year^{-1} from the cluster mean proper motion. Any star with an identified potential host cluster is then discarded from our analysis of wide binaries.

In general this procedure removes all the stars which

were otherwise found to have large number of detected companions, with only a single exception of the HD 183058 stars which is found to have 17 companions (separations less than 5 pc) around it with similar parallaxes and proper motions. We additionally checked the WEBDA catalogue (Mermilliod 1995) for this star. The star lacks known cluster association. It therefore suggests that our analysis identifies a new previously unknown open cluster or a stellar stream. We exclude this star and its companions from our following analysis.

4 ULTRA-WIDE O/B-STARS

It is known that up to a half of all massive stars are born in binaries (Sana et al. 2012) of any separation (at least in the LMC massive clusters). Around ~ 10 per cent of low-mass stars are in triples and this fraction reaches even up to 35 per cent for B stars (Moe & Di Stefano 2017). The majority of stable triple stars form hierarchical systems with an inner compact pair and a distant companion. It is known that some triples survive the X-ray binary stage (see examples in Section 2). However, previous studies typically focused on binaries with smaller separations than considered here, and our study therefore complements our current understanding of the multiplicity of massive stars.

For our analysis we use the second Gaia data release (Gaia Collaboration et al. 2016, 2018) as well as the Simbad database and catalogue of Galactic O stars (Sota et al. 2011, 2014; Maíz Apellániz et al. 2016). Only O/B stars (O-B5 spectral types, see Appendix B for the ADQL requests) with measured V magnitude are chosen. Our initial list contains 1674 (B0-B5 stars) and 588 (O stars). After removing stars with problematic astrometric measurements according to the Gaia database we keep 1937 stars. Applying the method described above we get the results in Figure 1. In our search we identified 69 reliable wide binaries, see Table 1. We plot the distribution of parallaxes and apparent Gaia G magnitudes in Figure 2.

The distribution of projected separation is presented in Figure 3. We also tried to exclude all distant pairs to stars which already have a component at smaller angular separation.

When we run the cluster identification for the whole list of 1937 O/B stars we find that only 353 of them are in clusters. This seemingly small fraction of ≈ 18 per cent is mostly due to the short lifetimes of most stellar clusters and associations, as we briefly discuss in the following.

Most stars (70-90 percents) are initially formed in stellar cluster/associations embedded in giant molecular clouds (Lada & Lada 2003). Such clusters are not seen in optics and undetectable by Gaia. Only 4-7 per cent of embedded clusters survive the gas expulsion phase to become visible as open clusters or OB associations. In particular, the lifetime of small clusters (up to 1000 stars) is about 10-20 Myr, with the first 10 Myr spent in the gas-embedded stage. Moreover, since our sample is dominated by B stars (which lifetime is longer than the typical lifetime of visible clusters) it is not surprising to find the majority of observed OB stars in our sample in the field.

Our technique might also be a subject to following caveats: (1) some of the stars are in clusters/associations which have not been previously identified (see previous sec-

tion for example of HD 183058) and (2) although some of the OB stars are not hosted by currently identified clusters, they may still have gravitationally unbound neighbors in phase space from a birth cluster in the process of dissolving.

The inferred multiplicity rate for the field O/B stars is $69/(1937 - 353) \approx 4.4$ per cent. We estimate the variance for the mean estimator as $\sqrt{\hat{p}(1 - \hat{p})/n} \approx 0.5$ per cent, we therefore see a multiplicity rate of 0.044 ± 0.005 . We also estimate this fraction independently for O and B stars. For O stars outside of open cluster (48.5 per cent of all O stars in our sample) the multiplicity fraction is $6/198 = 3 \pm 1$ per cent. For B stars outside of open cluster (90 per cent of all B stars in our sample) the multiplicity fraction is 4.5 per cent.

In our sample, due to the luminosity limit, we are only sensitive to wide components of O, B, A, F, G and partly K stars (see the Hertzsprung-Russell diagram in Figure 4). In order to plot the Hertzsprung-Russell diagram we correct the magnitudes for extinction using the Green et al. (2018) map. In order to convert from $E(B-V)$ to A_G and $E(Bp-Rp)$ we use $R = 3.1$, $A_g/A_v = 0.9$ and $E(Bp - Rp)/E(B - V) = 1.5$ and use a general correction of 0.884 for all the reddening values obtained from the map. If the location of the star is not covered by the map, we decide not to correct for the reddening. We infer the masses using combined Padova stellar isochrones (stellar tracks from Marigo et al. 2017) for a stellar age of 2 and 10 Myr for stars more and less massive than $3.5 M_\odot$ with the Gaia DR2 photometric system as described by Evans et al. (2018).

The inferred mass distribution of primary and secondary stars is plotted in Figure 4. Some primaries might be misclassified, for example CD-49 4263 seems to have mass $1.4 M_\odot$ which is below B9. There are 6 primary stars with inferred masses less than $2 M_\odot$ in our sample. These are CD-49 4263, 2MASS J05065551-0321132, HD 225190, HD 344313, TYC 3986-3080-1 and V* V1671 Cyg.

Another effect which we see in the mass distribution is that the low-mass stars are missing ($M < 0.5 M_\odot$) as expected from our selection bias for detecting only higher luminosity companions. In order to get a rough estimate for the total multiplicity fraction, one can consider the non-trivial assumption that the companion mass-function continues to follow the Kroupa initial mass function (IMF) (Kroupa 2001) down to low-mass stars, below our detection limit. Under this assumption we identify our lowest detectable companion mass M_0 , above which the survey is complete. We then normalize the Kroupa IMF as to get the exact number of stars with masses more than M_0 . The number of stars with masses less than M_0 can then be extrapolated from the assumed companion IMF. Since the exact completeness cut-off is difficult to assess, we consider M_0 in the range of 0.8-1.5 M_\odot and find the corresponding multiplicity fraction ranges between 22 to 32 per cent. Roughly we can say that the extrapolated multiplicity fraction is about 27 ± 5 per cent. In reality the systematic uncertainty arising from our assumption of the companion IMF to continue to low-mass values, could be much larger.

For comparison, the wide multiplicity rate for low mass primaries is $9.1\% \pm 1.6\%$ found for multiplicity of primary G dwarfs with separations larger than 10^3 a.u. by Lépine & Bongiorno (2007) and is dominated by M-dwarf companions. In other words the ultra-wide binary fraction of massive stars might be 2-3 times higher than that of low-mass

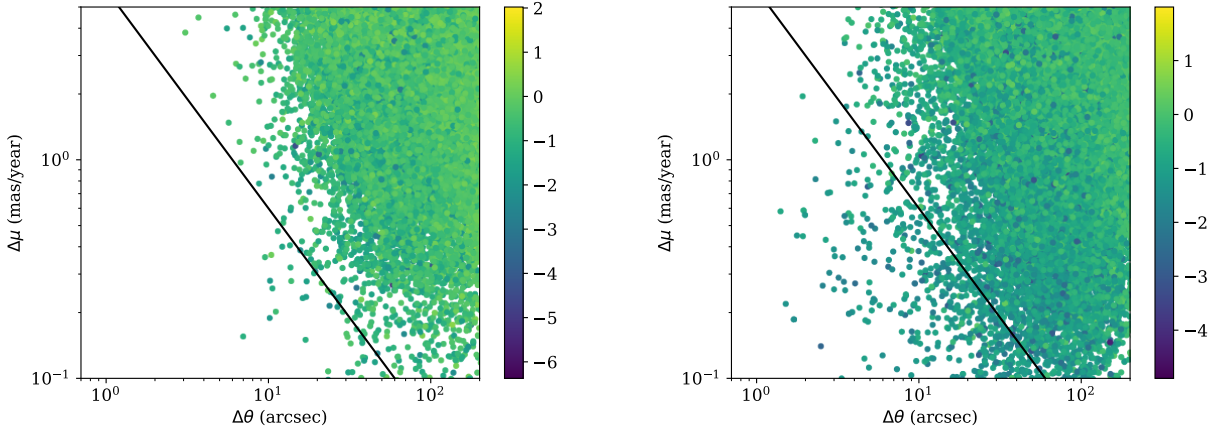


Figure 1. The difference in proper motion vs. the angular separation for the O/B-stars sample. Left panel: All the objects are shifted by $50'$ in the direction of declination as to exclude any possible real wide binaries from the mock-sample. Right panel: The observed distributions. The color shows the logarithm of the parallax difference. Black solid line assists comparison between the misplaced and observed sample.

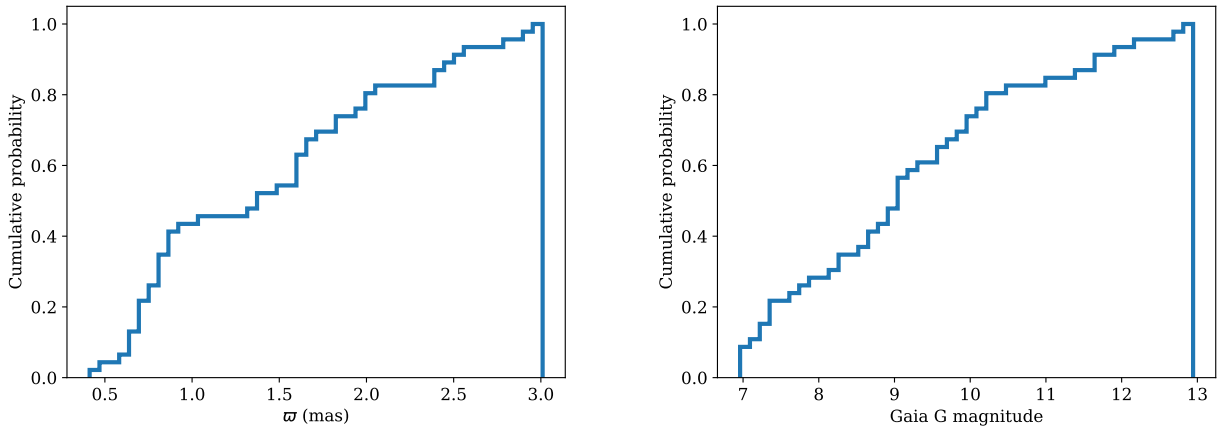


Figure 2. Cumulative distribution of parallaxes (left panel) and apparent G magnitude (right panel) for primary O/B stars with wide companions.

stars, a result consistent with theoretical expectations for dynamically-formed wide binaries where the ultra-wide binary fraction is expected to be much higher than that of low-mass stars (Perets & Kouwenhoven 2012). Since previous estimates of the multiplicity fraction of massive stars were limited to smaller separations than those considered here, this result hints a significant increase in the inferred multiplicity fraction of massive stars, with the majority being part of triple or higher multiplicity systems.

5 ULTRA-WIDE NS/BH SYSTEMS

We identify HMXBs and LMXBs in the second Gaia data release based on their optical magnitude (the exact procedure is described in Section 5.2). This approach does not work for normal and millisecond pulsars because of their faintness (the brightest object is the Crab pulsar with $V = 16.6$ mag, see Mignani 2011). Instead of following the same procedure

as for HMXBs and LMXBs, we try to identify normal pulsars and MSPs in the second Gaia data release based on position (circle of 3 arcsec around the radio position) and proper motion.

We failed to find any reliable (relative errors of parallax and proper motion measurements less than 0.25) optical counterpart for isolated normal radio pulsars based on their coordinate and proper motion. We have identified five optical counterparts (angular separation less than $3''$, similar proper motions) to MSPs, see Table E2. These pulsars and their optical counterparts are the same as found in Mingarelli et al. (2018) and Jennings et al. (2018), except for J1732-5049 and J1910+1256. Pulsar J1732-5049 does not have the timing measurement for parallax (Reardon et al. 2016), so it is difficult to verify this association. In the case of J1910+1256 the Gaia second data release provides only upper limit on the parallax and proper motion in the right ascension direction, so although we found the same association as in Mingarelli et al. (2018), we excluded this object. In

Name O/B star	Gaia primary Gaia DR2 name	Gaia secondary Gaia DR2 name	$\Delta\theta$ (arcsec)	$\Delta\varpi \pm \sigma_{\Delta\varpi}$ (mas)	$\Delta\mu \pm \sigma_{\Delta\mu}$ (mas year ⁻¹)	<i>A</i> (a.u.)
2MASS J05065551-0321132	3213014868922447232	3213015148092614656	120.9	0.116 ± 0.071	0.195 ± 0.096	48071.9
2MASS J05065551-0321132	3213014868922447232	3213016007087564160	229.9	0.088 ± 0.046	0.316 ± 0.085	91444.7
2MASS J05065551-0321132	3213014868922447232	3213010750047595520	281.1	0.022 ± 0.042	0.065 ± 0.076	111789.6
2MASS J05065551-0321132	3213014868922447232	3213010509529424384	389.5	0.058 ± 0.074	0.05 ± 0.094	154913.3
2MASS J05065551-0321132	3213014868922447232	3212957664251821824	443.3	0.066 ± 0.044	0.06 ± 0.082	176322.3
BD+50 377	358015279655161088	358009442797341568	119.4	0.101 ± 0.084	0.139 ± 0.135	48529.1
BD+50 377	358015279655161088	358009339718126720	136.4	0.085 ± 0.063	0.24 ± 0.107	55417.4
CD-44 11306	5964099137533440640	5964099343691734016	46.8	0.091 ± 0.067	0.117 ± 0.102	60453.3
CD-44 11306	5964099137533440640	5964098897015324928	103.2	0.091 ± 0.063	0.085 ± 0.12	133261.6
CD-44 11306	5964099137533440640	5964099446770967424	153.1	0.117 ± 0.066	0.058 ± 0.119	197566.0
CD-49 4263	5325671971449181696	5325671971449183488	16.5	0.013 ± 0.055	0.047 ± 0.099	39505.6
CD-49 4263	5325671971449181696	5325672761723170176	52.6	0.04 ± 0.045	0.027 ± 0.079	126113.8
HD 20508	462485965385240832	462482838649050496	124.4	0.08 ± 0.056	0.12 ± 0.076	151438.2
HD 21650	237762796737339776	237739191597107456	139.5	0.038 ± 0.109	0.203 ± 0.159	46341.3
HD 24190	218790861034319744	218791376433618304	156.0	0.115 ± 0.058	0.414 ± 0.123	64369.3
HD 33090	3414941966067063552	3414941966069295744	9.0	0.059 ± 0.065	0.104 ± 0.105	4417.8
HD 45677	2999967452909563136	2999967074952442624	29.4	0.01 ± 0.083	0.089 ± 0.135	18369.1
HD 52533	3108642147107724544	3108641773451669376	11.3	0.01 ± 0.071	0.117 ± 0.107	21915.9
HD 154538	5926578921730646144	5926578986111699712	9.9	0.034 ± 0.071	0.469 ± 0.111	6942.3
HD 155606	5953022382536807424	5953021690999065856	125.5	0.118 ± 0.084	0.083 ± 0.131	137246.6
HD 157020	5953355220976166016	5953355225327896064	43.1	0.039 ± 0.085	0.111 ± 0.14	52858.9
HD 158724	5974604764982749440	5974604558791120640	8.9	0.11 ± 0.074	0.203 ± 0.1	6418.4
HD 158724	5974604764982749440	5974604760652216320	44.0	0.04 ± 0.087	0.219 ± 0.146	31910.9
HD 162418	4036689403295912704	4036688548653697664	75.8	0.082 ± 0.081	0.08 ± 0.103	90670.4
HD 162540	4063721931768310528	4063721893097768320	56.8	0.102 ± 0.079	0.259 ± 0.147	32324.1
HD 162540	4063721931768310528	4063721313293010560	229.0	0.17 ± 0.088	0.161 ± 0.155	130264.2
HD 163393	4056195293667038592	4056195224947573760	75.4	0.106 ± 0.103	0.025 ± 0.152	129469.4
HD 164950	4064121913535676160	4064125143351139840	138.3	0.04 ± 0.062	0.05 ± 0.096	187113.1
HD 167474	4097483776326830720	4097483776326831744	23.7	0.03 ± 0.076	0.106 ± 0.115	33060.0
HD 169675	4096208514732308864	4096208372898138880	86.6	0.124 ± 0.073	0.179 ± 0.108	51630.3
HD 170051	4585303172501204480	4585315778226217728	393.7	0.032 ± 0.05	0.247 ± 0.068	135849.8
HD 170051	4585303172501204480	4584923566112188672	532.2	0.094 ± 0.066	0.103 ± 0.102	183648.8
HD 170051	4585303172501204480	4584939955707538560	541.2	0.063 ± 0.049	0.141 ± 0.082	186741.1
HD 171348	4079494769740363136	4079494769740368640	11.4	0.049 ± 0.085	0.098 ± 0.113	10912.7
HD 177648	4521438177054351104	4521414709351870720	12.4	0.033 ± 0.058	0.396 ± 0.08	7576.1
HD 179126	4264306623991981952	4264301577449116544	251.9	0.056 ± 0.086	0.046 ± 0.105	152349.1
HD 185418	4322021849109320320	4322021844762504064	12.5	0.058 ± 0.048	0.22 ± 0.068	9410.6
HD 186363	4239724640671288960	4239722922684335488	227.0	0.063 ± 0.074	0.228 ± 0.127	134856.5
HD 213023A	2205471994328733568	2205471998624679040	1.8	0.053 ± 0.058	0.452 ± 0.074	1827.6
HD 213023A	2205471994328733568	2205472307866244992	75.7	0.077 ± 0.041	0.183 ± 0.063	77397.1
HD 217086	2207291656008154112	2207269562701436160	229.0	0.023 ± 0.048	0.119 ± 0.081	195042.4
HD 217817	2013630893446412672	2013618828875520512	161.8	0.035 ± 0.081	0.195 ± 0.13	79268.7
HD 220598	1913545407978693632	1913543483833350528	258.5	0.078 ± 0.091	0.238 ± 0.108	106662.6
HD 225190	420276126312352896	420276981005904128	161.6	0.112 ± 0.11	0.364 ± 0.14	63115.7
HD 225190	420276126312352896	420298253984619520	417.8	0.087 ± 0.05	0.191 ± 0.07	163181.3
HD 225190	420276126312352896	420298013466438912	495.7	0.025 ± 0.118	0.209 ± 0.151	193605.8
HD 226609	2072510634482203520	2072510634482203136	3.2	0.055 ± 0.041	1.193 ± 0.073	1149.9
HD 235523	2172465655999346432	2172465759071547648	91.4	0.037 ± 0.045	0.251 ± 0.074	49480.0
HD 237121	461841342334222592	461841101815943936	100.6	0.115 ± 0.114	0.114 ± 0.156	121025.4
HD 248903	3444121565857570560	3444122321771813632	68.8	0.053 ± 0.087	0.036 ± 0.126	166820.7
HD 248903	3444121565857570560	3444121290979664256	70.4	0.117 ± 0.079	0.064 ± 0.107	170759.8
HD 248903	3444121565857570560	3444122351833299968	81.1	0.113 ± 0.082	0.028 ± 0.108	196568.3
HD 252532	3425061463071277184	3425061458773888512	12.4	0.011 ± 0.043	0.084 ± 0.072	24446.6
HD 282430	158645612194039808	158645612195930624	4.2	0.018 ± 0.081	0.395 ± 0.148	6184.7
HD 312640	4095537262805235072	4095537017965216384	104.8	0.014 ± 0.069	0.082 ± 0.116	153882.7
HD 314057	4093933448976732160	4093933586410393216	117.0	0.087 ± 0.101	0.1 ± 0.138	129831.8
HD 314057	4093933448976732160	4093934381021176448	143.5	0.086 ± 0.091	0.022 ± 0.14	159232.5
HD 328064	5990524898748290048	5990545381493482880	129.2	0.105 ± 0.071	0.024 ± 0.091	189741.9
HD 328907	5964302267984622336	5967281158540457600	166.6	0.079 ± 0.09	0.102 ± 0.146	180995.2
HD 329213	5964098720895565440	5964099343691734016	160.4	0.077 ± 0.071	0.069 ± 0.131	170197.2
HD 344313	2019268531933154176	2019267093154924416	104.2	0.02 ± 0.04	0.11 ± 0.063	56755.5
LB 3357	4668594889152178304	4668594889152178560	6.6	0.019 ± 0.028	0.208 ± 0.054	9001.4
TYC 3728-530-1	449218983208306304	449218983208307200	5.2	0.048 ± 0.073	0.224 ± 0.091	6515.5
TYC 3986-3080-1	2005104898028283520	2005104936694779264	59.3	0.016 ± 0.055	0.128 ± 0.091	81001.3
TYC 3986-3080-1	2005104898028283520	2005104799255829504	66.2	0.013 ± 0.057	0.073 ± 0.1	90435.5
V* IS Nor	5932588474413552512	5932588474413551488	2.5	0.002 ± 0.046	0.141 ± 0.07	1519.5
V* V1671 Cyg	2032810465079954944	2032810224561748480	160.5	0.103 ± 0.068	0.230 ± 0.117	104972.5
V* V730 Cep	2013474586693428096	2013474659716546688	150.1	0.004 ± 0.088	0.106 ± 0.128	72220.1
V* V730 Cep	2013474586693428096	2013474659716547968	154.0	0.037 ± 0.065	0.183 ± 0.1	74051.9

Table 1. Wide binaries found in the O/B sample. *A* is the projected orbital separation.

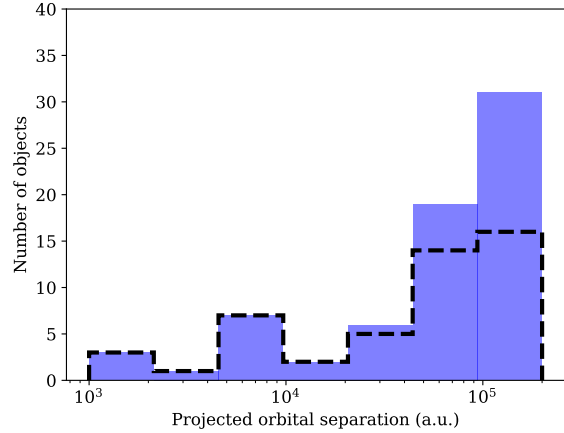
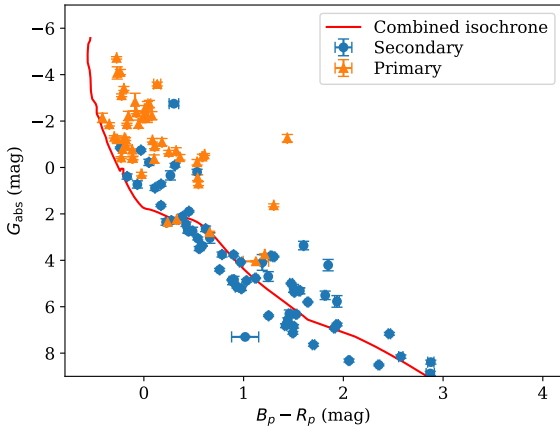


Figure 3. The Hertzsprung - Russell diagram (left panel) and the distribution of the observed spatial separations (right panel) for the wide astrometric pairs found in the O/B-stars sample. The blue (top filled) histogram corresponds to the separation of all candidates from the Table 1, and the black dashed histogram corresponds to the cases where only the closest component was selected in each case where more than a single companion was identified. The isochrone is combined from 2 Myr and 10 Myr isochrones for stars more massive and less massive than $3.5 M_{\odot}$ respectively.

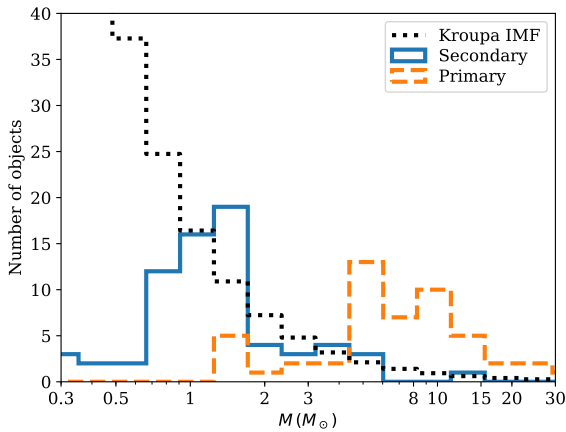


Figure 4. Distribution of masses of primaries and secondaries found in the O/B stellar sample. The dotted black line shows the Kroupa IMF consistent with mass distribution of secondaries more massive than $1.3 M_{\odot}$.

any case the number and quality of the Gaia measurements for MSPs counterparts prevent us from using these parallaxes and proper motions to search for wide pairs. Therefore, instead, we use the measurements of the parallaxes and proper motions obtained from radio observations of pulsars to search for possible second/third components in the optical data from Gaia. This approach is justified, since both the timing and the interferometric proper motion measurements as well as the Gaia measurements are all performed in the ICRF.

5.1 Data sources for normal and millisecond radio pulsars

For the normal radio pulsars we use the interferometric measurements of the parallax and proper motion based on several previous works: Briskin et al. (2002, 2003b); Chatterjee et al. (2001, 2004, 2009); Deller et al. (2009, 2018); Kirsten et al. (2015). To filter this list, we select only pulsars with relative error in parallaxes and proper motions less than 0.25. All of the selected objects and their measurements are compiled and shown in Table D1. In cases where a measurement has some asymmetric uncertainties, we use the largest uncertainty value. In total our list contains 57 pulsars. A priori we do not expect to find any wide astrometric pairs because the spatial velocities of these pulsars exceed 40 km s^{-1} (the velocity dispersion of NS progenitors is $10\text{--}15 \text{ km s}^{-1}$) except for PSR J0614+2229 which has a velocity of $\approx 20 \text{ km s}^{-1}$.

For the MSPs we prepared the sample using the interferometric measurements from several previous studies: Chatterjee et al. (2009); Deller et al. (2008); Deller et al. (2012, 2013); Yan et al. (2013) and collected the timing measurements from the following studies: Arzoumanian et al. (2018); Desvignes et al. (2016); Freire et al. (2012); Guillemot et al. (2016); Ng et al. (2014); Reardon et al. (2016); Stovall et al. (2014). The vast majority of the MSP measurements are timing ones obtained from Arzoumanian et al. (2018). In our sample we kept only objects with relative error of parallax and proper motion of less than 0.25. The list of pulsars together with their measurements is shown in Table E1. It contains 21 MSPs, some of these objects have very small spatial velocities. In order to simplify our analysis, we use the proper motion measurements in the equatorial coordinate system, even though the measurements in the ecliptic system might be more precise.

5.2 Data sources for XRBs

For our analysis we use two catalogues: Liu et al. (2006) for HMXBs (114 entries) and Liu et al. (2007) for LMXBs (187

entries) additionally checking details in the Simbad database (Wenger et al. 2000). The Simbad database includes all objects from both of these catalogues and newer measurements.

To choose only Galactic XRBs, we make use of the hierarchy information from `h_link` table in Simbad. We prepare our master list using ADQL query (Osuna et al. 2008, see Appendix B for details) selecting objects with type HMXB or LMXB and measured magnitude in V filter. Additionally we go through the list of all objects which are mentioned in the catalogues but have different type in the Simbad database. There are 25 objects which were classified as HMXBs in Liu et al. (2006), but their type is different in the Simbad database. We found that these objects were most probably mis-classified before, e.g. V* V4641 Sgr mentioned as HMXB in Liu et al. (2006) is classified as LMXB according to MacDonald et al. (2014) with the secondary mass $M_* = 2.9 \pm 0.4 M_\odot$; 2S 0053+604 appears to be Be star with an unusual X-ray emission properties (Robinson et al. 2002), V* RT Cru seems to be a symbiotic star according to Belczyński et al. (2000) and later works.

The cases of mis-classification or dubious classification are quite common for XRBs, because type identification requires long observations in multiple spectral ranges. We are interested in genuine XRBs with BH or NS companions, therefore we rely on the modern classification provided by the Simbad database.

A list of HMXBs based on the Simbad database appeared to have one extragalactic object: NGC 300 X-1 which was excluded manually. New XRBs were discovered since the publication of Liu et al. (2006) and Liu et al. (2007), and therefore the total number of Galactic XRBs with known V magnitude is 165 (HMXBs) and 57 (LMXBs). According to the Simbad database 44 HMXBs do not have V magnitude measurements. We tried to identify HMXBs based on their Gaia colors and absolute magnitude, but we were able to find only one system, CXOU J162046.2-513006 in the catalogue, see Appendix C.

5.2.1 Identification of the XRB sample in the Gaia dataset

Our XRB identification is based on spatial coincidence and magnitude similarity. We had to choose both criteria, since in a small region of a few arcsec (comparable to the size of point spread function of e.g. *XMM-Newton*), the second Gaia data release might contain up to tens of stars. The situation is especially difficult with the HMXBs which are typically found in star formation regions.

The magnitude could provide a reliable additional information to facilitate the identification of HMXBs because their intrinsic colors and absolute magnitudes differ significantly from that of the background M/K stellar population. In the case of LMXBs the situation is more complicated, since their optical emission is dominated by the accretion disk. The periodic optical variability and magnitude variation due to on/off state in the LMXBs could also have prevented us in some cases from correctly identifying them. In particular, in the case of V* V1727 Cyg the amplitude of the photometric variations reaches $\Delta B = 1.5$ mag. Our identification suggests that $D \approx 2$ kpc, a distance which is inconsistent with the claimed spectral type F of the stars according to Cowley & Schmidtke (1990).

Practically, we searched for all stars in the Gaia database within a $15''$ cones around the XRBs locations. For six out of 165 HMXB and 13 out of 57 LMXBs there are no optical counterparts with similar magnitudes at the location provided by the catalogues or Simbad. Our main test for the successful identification is a comparison of the V magnitude with the Gaia g magnitude. For objects with $B - V = 0$ (A2V spectral type) the unabsorbed $g \approx V$ according to Jordi et al. (2010). For B2V (common HMXB optical counterpart) stars the expected unabsorbed $g - V \approx -0.05$, while for G5V stars $g - V = -0.25$. The interstellar reddening can significantly change this value, that is why we allow $|g - V| < 1.5$ as a confirmation of positive identification. We assume that a star at the smallest separation from the expected coordinate with the $|g - V| < 1.5$ is the best counterpart for the XRB.

The six HMXBs which were not identified are:

- (i) 4U 1954+31 ($g - V \approx -1.6$ expected -1.45 based on $B - V$, but within uncertainty of Jordi et al. 2010 equation),
- (ii) SXP 4.78 no candidates brighter than $g = 17.33$ in $15''$ circle of its position although $B - V = 0.1$ and $V = 15.8$
- (iii) EM* VRMF 55, the candidate with $g - V = -2$ is difficult to verify since B is not measured
- (iv) AX J0048.2-7309, the candidate with $g - V = 2.13$ is difficult to verify since B is not measured
- (v) KRL2007b 348, the color $B - V = 1.62$ should correspond to $g - V \approx -0.97$ while in reality 1.64
- (vi) INTEGRAL1 111, the color $B - V = 2.2$ should correspond to $g - V \approx -1.63$ while actual $g - V \approx 1.8$

The list of LMXBs with the magnitude identification problems looks quite similar and we therefore do not show it here.

From our compiled list of XRBs with the Gaia counterpart we selected only objects with relative errors in parallax $\sigma_\varpi/\varpi < 0.25$ and proper motions $\sigma_\mu/\mu_\alpha < 0.25$ and $\sigma_\mu/\mu_\delta < 0.25$. Additionally we checked the quality of the astrometric solution following Lindgren et al. (2018). The final list consists of 28 HMXBs and 7 LMXBs, see Table 2.

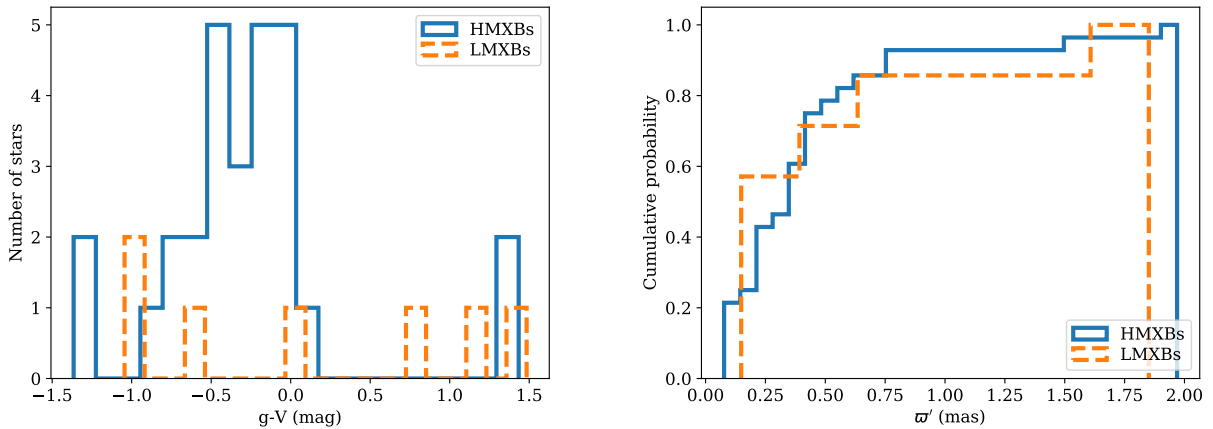
We show the distribution of parallaxes and $g - V$ colors in Figure 5. The mean parallax for the 28 HMXBs is 0.44 mas and the mean g magnitude is 10.78. There are two outliers with positive $g - V$ at this plot which is not expected. These two HMXBs are UCAC2 4813819 and AX J1739.1-3020, we believe these might be misidentified.

The mean parallax of seven LMXBs is 0.56 mas and the mean g magnitude is 14.16. The main reason why we have such a limited statistics for LMXBs is that the second Gaia data release does not have precise astrometric solution for the majority of LMXBs, likely because LMXBs are faint and are strongly variable in the optical band. We find three outliers with unexpected color $g - V > 0$: V* V1727 Cyg, V* GU Mus and V* IL Lup.

5.3 Results

We found no reliable wide astrometric pairs of XRB or MSP or pulsar and a field star. We show the distribution of angular separations and differences in proper motions in Figures 6 and 7. Below we analyze and discuss in more details the statistical significance of these results.

HMXB	Sp. type	Gaia counterpart Gaia DR2 ID	V (mag)	g (mag)	$\varpi \pm \sigma_\varpi$ (mag)	$\mu_\alpha \pm \sigma_\alpha$ (mas / year)	$\mu_\delta \pm \sigma_\delta$ (mas/year)
HD 100199	B0/1(III)n(e)	5333660129603575808	8.17	8.13	0.769 ± 0.069	-6.202 ± 0.109	1.296 ± 0.099
GRO J2058+42	O9.5-B0IV-Ve	2065653598916388352	14.74	14.19	0.077 ± 0.018	-2.219 ± 0.033	-3.356 ± 0.031
LS 1698	B0III/V:e	5352018121173519488	11.48	11.25	0.156 ± 0.034	-6.265 ± 0.062	2.821 ± 0.057
UCAC2 4813819	B2III/B0V	5335021599905643264	13.4	14.75	0.236 ± 0.027	-3.464 ± 0.039	1.18 ± 0.04
KRL2007b 84	B0e	5258414192353423360	15.27	13.9	0.244 ± 0.033	-4.844 ± 0.064	3.546 ± 0.055
GSC 03588-00834	B0Ve	2162805896614571904	14.2	13.76	0.116 ± 0.019	-3.533 ± 0.031	-3.172 ± 0.028
HD 34921	B0IVpe	184497471323752064	7.48	7.22	0.753 ± 0.057	1.444 ± 0.118	-4.116 ± 0.07
AX J1700.2-4220	Be	5966213219190201856	9.15	8.68	0.616 ± 0.063	1.214 ± 0.123	-1.42 ± 0.096
AX J1739.1-3020	O8.5Iab(f)	4056922100878037120	14.8	16.23	0.651 ± 0.068	2.887 ± 0.112	1.732 ± 0.087
BD+53 2790	O9.5Vep	2005653524280214400	9.84	9.74	0.267 ± 0.03	-4.256 ± 0.058	-3.11 ± 0.048
V* V572 Pup	B0.2IVe	5548261400354128768	12.74	12.48	0.103 ± 0.024	-1.575 ± 0.037	2.149 ± 0.045
HD 249179	B5ne	3431561565357225088	10.0	10.01	0.387 ± 0.057	0.61 ± 0.108	-2.716 ± 0.087
V* GP Vel	B0.5Ia	5620657678322625920	6.87	6.72	0.384 ± 0.03	-4.963 ± 0.052	9.092 ± 0.052
SS 188	OB	5541793213959987968	12.33	12.17	0.1 ± 0.025	-2.558 ± 0.039	3.08 ± 0.044
V* V479 Sct	O(f)N6.5V	4104196427943626624	11.27	10.8	0.484 ± 0.052	7.428 ± 0.088	-8.0 ± 0.069
BD+60 73	B1Ib	427234969757165952	9.66	9.45	0.274 ± 0.031	-1.801 ± 0.043	-0.366 ± 0.039
EM* AS 14	B2	414196617287885312	11.36	11.43	0.367 ± 0.029	-2.298 ± 0.037	-0.549 ± 0.039
4U 2238+60	Be	2201091578667140352	14.8	14.15	0.084 ± 0.019	-2.393 ± 0.032	-1.045 ± 0.03
IGR J01583+6713	B2IVe+	518990967445248256	14.43	13.7	0.098 ± 0.018	-1.144 ± 0.024	0.298 ± 0.03
HD 74194	O8.5Ib-II(f)p	5522306019626566528	7.55	7.44	0.424 ± 0.03	-7.453 ± 0.056	5.805 ± 0.048
HD 63666	B7IV/V	5489434710755238400	7.6	7.52	1.529 ± 0.043	-4.528 ± 0.088	8.596 ± 0.086
WRAY 15-793	O9.5III/Ve	5336957010898124160	12.12	11.6	0.313 ± 0.027	-5.387 ± 0.04	1.301 ± 0.037
HD 49798	sdO6	5562023884304074240	8.287	8.21	1.969 ± 0.064	-4.11 ± 0.113	5.669 ± 0.118
V* BP Cru	B1.5Iaeq	6054569565614460800	10.66	9.76	0.253 ± 0.035	-5.303 ± 0.051	-2.166 ± 0.049
HD 245770	O9/B0III/Ve	3441207615229815040	9.39	8.68	0.442 ± 0.049	-0.628 ± 0.09	-3.036 ± 0.066
IGR J17544-2619	O9Ib	4063908810076415872	12.94	11.67	0.352 ± 0.05	-0.65 ± 0.084	-0.534 ± 0.066
HD 226868	O9.7Iabpvar	2059383668236814720	8.91	8.52	0.422 ± 0.032	-3.882 ± 0.048	-6.171 ± 0.054
CPD-63 2495	O9.5Ve	586229960127967488	9.98	9.63	0.418 ± 0.031	-6.986 ± 0.043	-0.416 ± 0.044
LMXB							
V* V1727 Cyg		1978241050130301312	16.4	17.6	0.547 ± 0.092	-2.301 ± 0.156	-4.392 ± 0.152
V* GU Mus	K3V-K7V	5234956524094035840	13.3	14.78	0.165 ± 0.023	-3.085 ± 0.039	0.463 ± 0.035
V* V934 Cen	M2III	6158386896580577152	7.85	6.91	1.851 ± 0.063	-39.583 ± 0.103	-6.028 ± 0.144
V* V1333 Aql		4264296560926758144	14.8	14.2	0.186 ± 0.043	-5.009 ± 0.089	-6.141 ± 0.069
V* HZ Her	B3/6ep	1338822021487330304	13.63	13.61	0.149 ± 0.027	-1.267 ± 0.047	-7.91 ± 0.053
V* IL Lup	A2V	5986117923045613184	14.9	15.73	0.314 ± 0.044	-7.221 ± 0.087	-2.971 ± 0.064
PSR J1023+0038	GV	3831382647922429952	17.31	16.27	0.728 ± 0.143	4.751 ± 0.135	-17.348 ± 0.135

Table 2. Catalogue of XRBs with their Gaia counterparts with well measured parallaxes and proper motions.**Figure 5.** Left panel: The distribution of observed colors for the XRBs matched with their Gaia counterparts. Right panel: The cumulative distribution of parallaxes for the Gaia counterparts of XRBs.

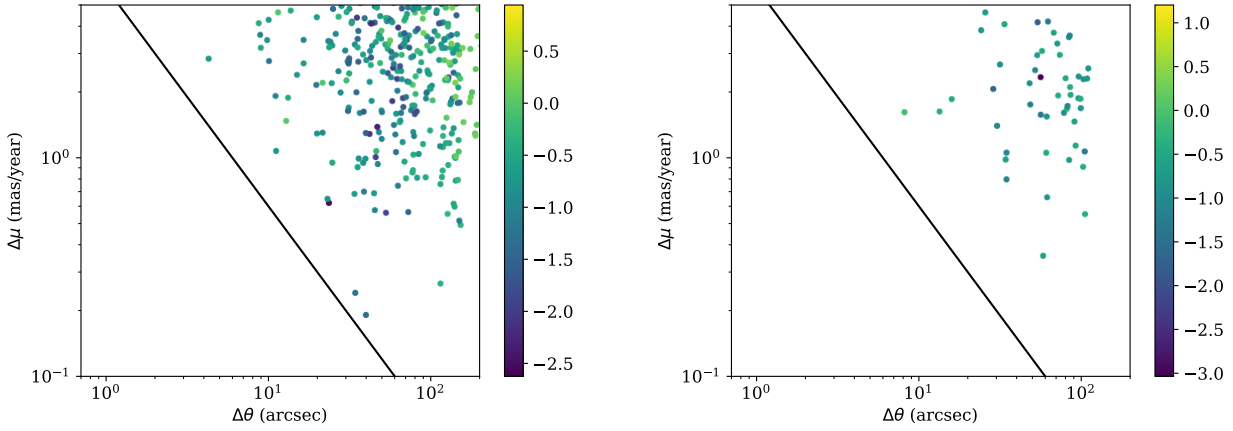


Figure 6. The differences in proper motions vs. the angular separation for HMXBs (left panel) and LMXBs (right panel). The color shows the logarithm of parallax difference.

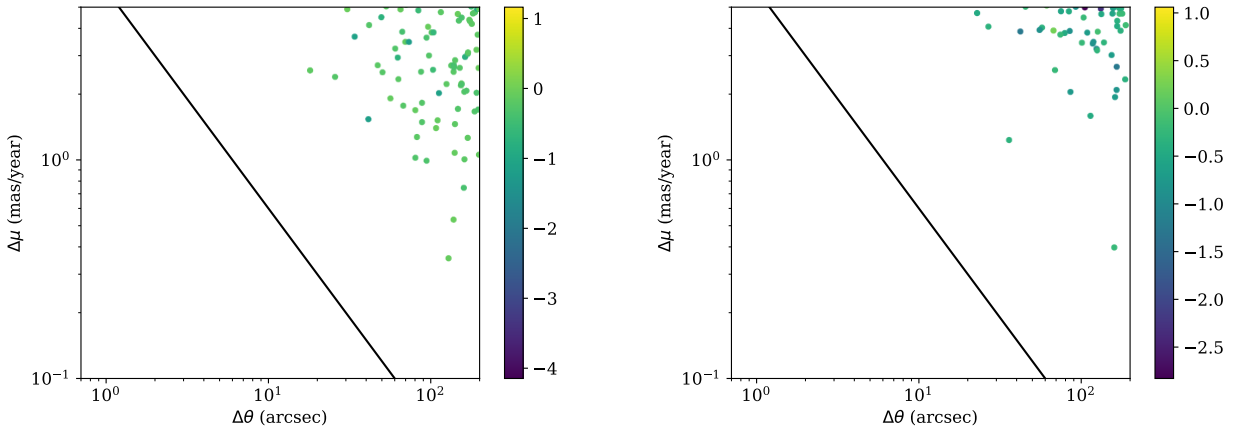


Figure 7. The differences in the proper motions vs. the angular separation of PSRs (left panel) and MSPs (right panel). The color shows the logarithm of the parallax difference.

5.4 Constraints on fraction of weak natal kicks

The direct comparison of the verification sample (O/B stars) with the non detection of reliable wide components of XRBs is not straightforward because some of the OB stars from the verification sample are isolated while all XRBs were originally binaries (we neglect here the dynamical formation in the field). To take this effect into account we have to rely on stellar statistics. [Moe & Di Stefano \(2017\)](#) provides the following fraction of isolated, binary, triple and quadruple stars for primaries of $10 M_{\odot}$: 17.5%, 35%, 30%, 17.5%. If we neglect stellar interactions, progenitors of HMXBs were binaries in 42%, triples in 36% and quadruples in 22% of cases. If none of the compact objects received a natal kick (which is known not to be the case) and the mass loss was adiabatic, such the third component could survive, we would have expected it that 58% of HMXBs should have one or two bound companions. For a sample of early B stars the second, third or fourth component should have been identified in 83% of the cases. This would suggest that a wide companion should

be identified 1.4 times more often in the sample of B stars than in sample of binary B stars.

Using the hypergeometric distribution we can compute how significant is it not to find any distant companions to HMXBs. We re-scale the fraction 0.044 to $0.044/1.4 \approx 0.03$. For the moment let us assume that the total sample size is 165 objects (if we double the sample size it does not change the probability significantly). In this case the probability to find no distant companion is 0.39 and the probability to find a single distant component is 0.41. If we assume that only 10 percent of NSs receive sufficiently small natal kicks to keep their wide companions then the probability to find no distant components becomes 0.92 and a probability to find one distant component is 0.08.

At the moment the XRBs sample is too small to constrain the weakest natal kick through the suggested method. Future increase in the size of XRB sample in the Gaia will let us to constrain this hypothesis much better.

As for the normal radio pulsars, the probability to find no wide pairs among 57 pulsars is 0.07 (if the fraction of weak kicks is 100 per cent) which independently shows that most

NSs receives strong natal kick. If the NSs receives weak natal kick in 10 per cent of the cases, non detection of ultra-wide pairs is compatible with expectations (0.83 probability to find none ultra-wide pair and 0.17 probability to find single ultra-wide pair).

As for millisecond radio pulsars the probabilities are: non detection has probability 0.5 (assuming 100 per cent fraction of weak kicks) and 0.93 (assuming 10 per cent fraction of weak kicks).

6 DISCUSSION AND SUMMARY

Using the second Gaia data release, we identified and characterized the population of ultra-wide massive OB binaries. We find that 4.4 ± 0.5 per cent of O-B5 stars have ultra-wide ($10^3 - 2 \times 10^5$ AU) companions down to the detection limit (G-stars).

In addition, we searched for astrometric wide companions to NS/BH binaries, by searching for third companions to HMXB, LMXB or MSP binaries or wide companions to normal radio pulsars. Since such wide binaries would be disrupted if the compact object received a natal kick larger than a few km s^{-1} , any finding of such wide binaries would provide a potential strong evidence for the existence of ultra-low or even zero-velocity natal kicks, while null finding could provide constraints on the fraction of systems that could receive such low-kicks.

Finally, we note that the third Gaia data release will enable us to probe the lowest NS and BH natal kicks using the same approach, but the better data will be sufficient to provide a much better statistically significant results and probe a larger sample of XRBs.

ACKNOWLEDGEMENTS

A.I. thanks Evgeni Grishin and Yonadav Bary Ginat for useful discussions. A.I. and H.P. thanks anonymous referee for useful comments.

This work has made use of data from the European Space Agency (ESA) mission *Gaia* (<https://www.cosmos.esa.int/gaia>), processed by the *Gaia* Data Processing and Analysis Consortium (DPAC, <https://www.cosmos.esa.int/web/gaia/dpac/consortium>). Funding for the DPAC has been provided by national institutions, in particular the institutions participating in the *Gaia* Multilateral Agreement.

This research has made use of the SIMBAD database, operated at CDS, Strasbourg, France

REFERENCES

- Abt H. A., 1983, *ARA&A*, **21**, 343
 Andrews J. J., Chanamé J., Agüeros M. A., 2017, *MNRAS*, **472**, 675
 Arzoumanian Z., et al., 2018, preprint, ([arXiv:1801.01837](https://arxiv.org/abs/1801.01837))
 Bassa C. G., et al., 2016, *MNRAS*, **460**, 2207
 Belczyński K., Mikołajewska J., Munari U., Ivison R. J., Friedjung M., 2000, *A&AS*, **146**, 407
 Bhattacharya D., van den Heuvel E. P. J., 1991, *Phys. Rep.*, **203**, 1
 Binney J., Tremaine S., 2008, *Galactic Dynamics: Second Edition*. Princeton University Press
 Bothwell M. S., Torres M. A. P., Garcia M. R., Charles P. A., 2008, *A&A*, **485**, 773
 Brisken W. F., Benson J. M., Goss W. M., Thorsett S. E., 2002, *ApJ*, **571**, 906
 Brisken W. F., Fruchter A. S., Goss W. M., Herrnstein R. M., Thorsett S. E., 2003a, *AJ*, **126**, 3090
 Brisken W. F., Thorsett S. E., Golden A., Goss W. M., 2003b, *ApJ*, **593**, L89
 Cantat-Gaudin T., et al., 2018, *A&A*, **618**, A93
 Chatterjee S., Cordes J. M., Lazio T. J. W., Goss W. M., Fomalont E. B., Benson J. M., 2001, *ApJ*, **550**, 287
 Chatterjee S., Cordes J. M., Vlemmings W. H. T., Arzoumanian Z., Goss W. M., Lazio T. J. W., 2004, *ApJ*, **604**, 339
 Chatterjee S., et al., 2009, *ApJ*, **698**, 250
 Cowley A. P., Schmidtke P. C., 1990, *AJ*, **99**, 678
 Deller A. T., Verbiest J. P. W., Tingay S. J., Bailes M., 2008, *ApJ*, **685**, L67
 Deller A. T., Tingay S. J., Bailes M., Reynolds J. E., 2009, *ApJ*, **701**, 1243
 Deller A. T., et al., 2012, *ApJ*, **756**, L25
 Deller A. T., Boyles J., Lorimer D. R., Kaspi V. M., McLaughlin M. A., Ransom S., Stairs I. H., Stovall K., 2013, *ApJ*, **770**, 145
 Deller A. T., et al., 2018, preprint, ([arXiv:1808.09046](https://arxiv.org/abs/1808.09046))
 Desvignes G., et al., 2016, *MNRAS*, **458**, 3341
 Duchêne G., Kraus A., 2013, *ARA&A*, **51**, 269
 Duquenois A., Mayor M., 1991, *A&A*, **248**, 485
 El-Badry K., Rix H.-W., 2018, *MNRAS*, **480**, 4884
 Evans D. W., et al., 2018, *A&A*, **616**, A4
 Freire P. C. C., et al., 2012, *MNRAS*, **423**, 3328
 Gaia Collaboration et al., 2016, *A&A*, **595**, A1
 Gaia Collaboration et al., 2018, *A&A*, **616**, A1
 Garcia M. R., Bailyn C. D., Grindlay J. E., Molnar L. A., 1989, *ApJ*, **341**, L75
 Giacobbo N., Mapelli M., 2019, *MNRAS*, **482**, 2234
 Green G. M., et al., 2018, *MNRAS*, **478**, 651
 Guillemot L., et al., 2016, *A&A*, **587**, A109
 Heggie D. C., 1975, *MNRAS*, **173**, 729
 Hobbs G., Lorimer D. R., Lyne A. G., Kramer M., 2005, *MNRAS*, **360**, 974
 Janka H.-T., 2013, *MNRAS*, **434**, 1355
 Janka H.-T., 2017, *ApJ*, **837**, 84
 Jennings R. J., Kaplan D. L., Chatterjee S., Cordes J. M., Deller A. T., 2018, *ApJ*, **864**, 26
 Jonker P. G., Nelemans G., 2004, *MNRAS*, **354**, 355
 Jordi C., et al., 2010, *A&A*, **523**, A48
 Kaplan D. L., et al., 2016, *ApJ*, **826**, 86
 Kirsten F., Vlemmings W., Campbell R. M., Kramer M., Chatterjee S., 2015, *A&A*, **577**, A111
 Kouwenhoven M. B. N., Goodwin S. P., Parker R. J., Davies M. B., Malmberg D., Kroupa P., 2010, *MNRAS*, **404**, 1835
 Kroupa P., 2001, *MNRAS*, **322**, 231
 Lada C. J., Lada E. A., 2003, *ARA&A*, **41**, 57
 Lai D., 2001, in Blaschke D., Glendenning N. K., Sedrakian A., eds, *Lecture Notes in Physics*, Berlin Springer Verlag Vol. 578, *Physics of Neutron Star Interiors*. p. 424 ([arXiv:astro-ph/0012049](https://arxiv.org/abs/astro-ph/0012049))
 Lépine S., Bongiorno B., 2007, *AJ*, **133**, 889
 Lin J., Nowak M. A., Chakrabarty D., 2009, *ApJ*, **706**, 1069
 Lindegren L., et al., 2018, *A&A*, **616**, A2
 Liu Q. Z., van Paradijs J., van den Heuvel E. P. J., 2006, *A&A*, **455**, 1165
 Liu Q. Z., van Paradijs J., van den Heuvel E. P. J., 2007, *A&A*, **469**, 807
 Livio M., Soker N., 1988, *ApJ*, **329**, 764
 Lyne A. G., Lorimer D. R., 1994, *Nature*, **369**, 127

- Lyne A. G., Stappers B. W., Keith M. J., Ray P. S., Kerr M., Camilo F., Johnson T. J., 2015, *MNRAS*, **451**, 581
- MacDonald R. K. D., et al., 2014, *ApJ*, **784**, 2
- Maíz Apellániz J., et al., 2016, *ApJS*, **224**, 4
- Manchester R. N., Hobbs G. B., Teoh A., Hobbs M., 2005, *AJ*, **129**, 1993
- Marigo P., et al., 2017, *ApJ*, **835**, 77
- Mermilliod J.-C., 1995, in Egret D., Albrecht M. A., eds, *Astrophysics and Space Science Library* Vol. 203, *Information On-Line Data in Astronomy*. pp 127–138, doi:10.1007/978-94-011-0397-8_12
- Mignani R. P., 2011, *Advances in Space Research*, **47**, 1281
- Mingarelli C. M. F., Anderson L., Bedell M., Spergel D. N., 2018, arXiv e-prints,
- Miyaji S., Nomoto K., Yokoi K., Sugimoto D., 1980, *PASJ*, **32**, 303
- Moe M., Di Stefano R., 2017, *ApJS*, **230**, 15
- Moeckel N., Bate M. R., 2010, *MNRAS*, **404**, 721
- Moeckel N., Clarke C. J., 2011, *MNRAS*, **415**, 1179
- Ng C., et al., 2014, *MNRAS*, **439**, 1865
- Nomoto K., 1984, *ApJ*, **277**, 791
- Nomoto K., 1987, *ApJ*, **322**, 206
- Nomoto K., Kondo Y., 1991, *ApJ*, **367**, L19
- Osuna P., et al., 2008, IVOA Astronomical Data Query Language Version 2.00, IVOA Recommendation 30 October 2008 (arXiv:1110.0503)
- Paczynski B., 1976, in Eggleton P., Mitton S., Whelan J., eds, *IAU Symposium Vol. 73, Structure and Evolution of Close Binary Systems*. p. 75
- Perets H. B., Kouwenhoven M. B. N., 2012, *ApJ*, **750**, 83
- Portegies Zwart S. F., Verbunt F., 1996, *A&A*, **309**, 179
- Portegies Zwart S., van den Heuvel E. P. J., van Leeuwen J., Nelemans G., 2011, *ApJ*, **734**, 55
- Raghavan D., et al., 2010, *ApJS*, **190**, 1
- Ransom S. M., et al., 2014, *Nature*, **505**, 520
- Reardon D. J., et al., 2016, *MNRAS*, **455**, 1751
- Repetto S., Davies M. B., Sigurdsson S., 2012, *MNRAS*, **425**, 2799
- Repetto S., Igoshev A. P., Nelemans G., 2017, *MNRAS*, **467**, 298
- Robinson R. D., Smith M. A., Henry G. W., 2002, *ApJ*, **575**, 435
- Sana H., et al., 2012, *Science*, **337**, 444
- Sota A., Maíz Apellániz J., Walborn N. R., Alfaro E. J., Barbá R. H., Morrell N. I., Gamen R. C., Arias J. I., 2011, *ApJS*, **193**, 24
- Sota A., Maíz Apellániz J., Morrell N. I., Barbá R. H., Walborn N. R., Gamen R. C., Arias J. I., Alfaro E. J., 2014, *ApJS*, **211**, 10
- Stovall K., et al., 2014, *ApJ*, **791**, 67
- Tauris T. M., 2011, in Schmidtbreick L., Schreiber M. R., Tapert C., eds, *Astronomical Society of the Pacific Conference Series* Vol. 447, *Evolution of Compact Binaries*. p. 285 (arXiv:1106.0897)
- Tauris T. M., van den Heuvel E. P. J., 2014, *ApJ*, **781**, L13
- Toonen S., Nelemans G., 2013, *A&A*, **557**, A87
- Toonen S., Nelemans G., Portegies Zwart S., 2012, *A&A*, **546**, A70
- Toonen S., Perets H. B., Igoshev A. P., Michaely E., Zenati Y., 2018, *A&A*, **619**, A53
- Verbunt F., Igoshev A., Cator E., 2017, *A&A*, **608**, A57
- Wenger M., et al., 2000, *A&AS*, **143**, 9
- Yan Z., Shen Z.-Q., Yuan J.-P., Wang N., Rottmann H., Alef W., 2013, *MNRAS*, **433**, 162
- de Kool M., 1990, *ApJ*, **358**, 189
- de Kool M., van den Heuvel E. P. J., Pylyser E., 1987, *A&A*, **183**, 47

APPENDIX A: THE LIFETIME OF ULTRA-WIDE BINARIES

It is worth discussing whether ultra-wide binaries could potentially be bound for a long time. According to Binney & Tremaine (2008) two type of objects play leading roles in the disruption of a wide binary: passing stars and molecular clouds. For the passing stars we get the following estimate:

$$t_d \approx 15 \text{ Gyr} \frac{k_{\text{diff}}}{0.002} \frac{10^4 \text{ a.u.}}{a} \frac{M_b}{2M_\odot} \quad (\text{A1})$$

where M_b is the total mass of the binary, the diffusion coefficient is $k_{\text{diff}} \approx 0.022/\ln \Lambda$ and $\ln \Lambda$ is:

$$\ln \Lambda \approx \ln \left\{ \frac{\sigma_{\text{rel}}^2 a}{GM_p} \right\} = 13.5 \quad (\text{A2})$$

where we assume the dispersion of relative velocity to be $\sigma_{\text{rel}} \approx 40 \text{ km s}^{-1}$ and mass of perturber to be $M_p = 1 M_\odot$ which means that a massive binary ($M_b = 20 M_\odot$) with semi-major axis of $2 \times 10^5 \text{ a.u.}$ can stay bound up to $\approx 6 \text{ Gyr}$. The effect of passing molecular clouds is much more severe:

$$t_d \approx 380 \text{ Gyr} \left(\frac{10^4 \text{ a.u.}}{a} \right)^3 \frac{M_b}{2M_\odot} \quad (\text{A3})$$

assuming similar values for the surface and volume density of giant molecular clouds as in Binney & Tremaine (2008) which results in a timescale of 0.5 Gyr for massive binary with orbital separation of 2×10^5 . It is known that massive B stars, HMXBs and normal radio pulsars can live for $\sim 10^7$ years. Therefore, such extra wide binaries could indeed be found.

APPENDIX B: ADQL REQUESTS

Here we show two ADQL requests for the Simbad database which helped us to form the initial HMXB lists before filtering:

```
SELECT main_id, ra, dec, V
FROM basic join allfluxes ON oid=oidref
WHERE otype = 'HMXB' and V is not Null
and oid NOT IN (SELECT child FROM h_link)
```

This is the request for the LMXB source list:

```
SELECT main_id, ra, dec, V
FROM basic join allfluxes ON oid=oidref
WHERE otype = 'LMXB' and V is not Null
and oid NOT IN (SELECT child FROM h_link)
```

We select massive stars (B0-B5) stars from the Simbad database with following query:

```
SELECT main_id, ra, dec, V
FROM basic join allfluxes ON oid=oidref
WHERE ((sp_type like 'B0%') or (sp_type like 'B1%')
or (sp_type like 'B2%') or (sp_type like 'B3%')
or (sp_type like 'B4%') or (sp_type like 'B5%'))
and V is not Null and V > 0 and plx_value > 0
and plx_err > 0 and plx_value/ plx_err > 4
and pm_err_maj > 0 and pmra / pm_err_maj > 4
and pm_err_maj > 0 and pmra / pm_err_maj > 4
and plx_value > 0.1
```

and oid NOT IN (SELECT child FROM h_link)
order by main_id

Below we show our ADQL request to select binary candidates to a particular massive star or remnant:

```
SELECT *
FROM (
SELECT source_id,ra, dec, parallax, parallax_error,
pmra, pmra_error, bp_rp, phot_g_mean_flux_over_error,
phot_bp_mean_flux_over_error, parallax_over_error,
pmdec, pmdec_error, phot_g_mean_mag,
astrometric_chi2_al, astrometric_n_good_obs_al,
DISTANCE(POINT('ICRS',ra,dec),
POINT('ICRS', RA, DEC)) AS dist,
abs(parallax - PAR) as dvarpi,
sqrt(power(parallax_error, 2) + PAR_ERR)
as sigma_delta_varpi,
sqrt(power(pmra - PRMT_RA, 2) +
power(pmdec - PRMT_DEC, 2))
as delta_mu, pmra - PRMT_RA as delta_mura,
pmdec - PRMT_DEC as delta_mudec,
1.0 / (sqrt(power(pmra - PRMT_RA, 2) +
power(pmdec - PRMT_DEC, 2))) *
sqrt( (power(pmra_error,2) + power(PRMT_RA_ERR, 2)) *
power(pmra - PRMT_RA, 2) +
(power(pmdec_error, 2.0) + power(PRMT_DEC_ERR,2))
* power(pmdec - PRMT_DEC, 2.0)) as sigma_delta_mu,
0.53 * power (parallax, 1.5)
/ sqrt(DISTANCE(POINT('ICRS',ra,dec),
POINT('ICRS', RA , DEC)) * 3600) as mu_orb
FROM gaiadr2.gaia_source
WHERE abs(parallax) / parallax_error > 3
and parallax > 0
and abs(pmra) / pmra_error > 3 and
sqrt(astrometric_chi2_al /
(astrometric_n_good_obs_al - 5))
< 1.2 * 0.5 *
((exp(-0.2 * (phot_g_mean_mag - 19.5)) + 1.0)
+ abs(exp(-0.2 * (phot_g_mean_mag - 19.5)) - 1.0))
and abs(pmdec) / pmdec_error > 3 ) as t
WHERE dvarpi < 2 * sigma_delta_varpi
and delta_mu < (mu_orb + 2 * sigma_delta_mu)
and sigma_delta_varpi < 0.12 and delta_mu < 3 * mu_orb
and sigma_delta_mu < 0.16
and 1=CONTAINS(POINT('ICRS',ra,dec),
CIRCLE('ICRS',RA , DEC , ANGLE ))
ORDER by dist
```

where RA, DEC, PAR, PAR_ERR, PRMT_RA, PRMT_DEC, PRMT_RA_ERR, PRMT_DEC_ERR are measured values for the primary star, namely: right ascension, declination, parallax, parallax error, proper motion in the right ascension direction and declination direction as well as their errors. ANGLE is the size of the requested area.

APPENDIX C: IDENTIFICATION OF HMXBS BASED ON COLOR

In order to increase statistical significance we tried to increase the sample of identified HXMBs based on color prop-

erties. To do so, we selected all Galactic HMXBs with no measured V magnitude:

```
SELECT main_id, ra, dec, V
FROM basic join allfluxes ON oid=oidref
WHERE otype = 'HMXB' and V is Null
and oid NOT IN (SELECT child FROM h_link)
```

After this, we checked colors and absolute magnitude (with no correction for reddening) of all stars in the second Gaia data release at angular separation of $15''$. We choose as potential candidates only stars with $-0.5 < B_p - R_p < 2$ and $-5 < g + 15 \log_{10} \varpi + 5.0 < 3$. These boundaries were found using the scattering of colors and absolute magnitudes of stars from our verification sample. Initial selection identified 13 candidates for 44 HMXBs and only one of them has good enough measurements of parallax and proper motion.

APPENDIX D: LIST OF NORMAL RADIO PULSARS

APPENDIX E: LIST OF MSPS

APPENDIX F: FORMATION OF ULTRA-WIDE BINARIES DUE TO A STRONG NATAL KICK

The strong natal kick could lead to a formation of ultra wide binary if it has preferable orientation and magnitude. For example, if the binary escape velocity is 100 km s^{-1} and the natal kick of neutron star is 99 km s^{-1} (assuming zero mass loss for a moment), it would lead to a formation of a binary with large semi-major axis and eccentricity close to 1. However, this happens quite infrequently. To check the likelihood for such formation channel we performed a binary stellar population synthesis using the code SeBa (Portegies Zwart & Verbunt 1996; Toonen et al. 2012; Toonen & Nelemans 2013).

In the modeling we mostly use the standard assumptions about the initial distribution of semi-major axis, eccentricities, initial masses and mass fractions, see e.g. Toonen et al. (2018). In particular we choose to model the distribution of semi-major axis following a flat distribution in logarithm of semi-major axis ranging from 0 till 1000 a.u. (Abt 1983). The smaller range is chosen to exclude initially wide systems which survived a weak natal kick. For primary star the mass ranges between 4 and 25 solar masses. The mass is chosen from the Kroupa mass function (Kroupa 2001). The secondary masses are drawn from flat distribution $0 < M_2/M_1 < 1$ (Duchêne & Kraus 2013). The initial eccentricities follow the thermal distribution (Heggie 1975).

We compute the evolution of stars for 60 Myr because we are primary interested in normal radio pulsars with ultra-wide companion. The lifetime of normal radio pulsar seems to be comparable to 10 Myr, the lifetime of lightest star which forms a neutron star in our simulations is ≈ 45 Myr. We choose to model two very different natal kick velocity distributions, namely the Verbunt et al. (2017) (model A) and Hobbs et al. (2005) (model B). The former one has significantly large fraction of weak natal kicks, while the later one has small number of weak natal kicks.

A fraction of close binaries goes through the common envelope evolution before or after the primary supernova

PSR name	$\varpi \pm \sigma_\varpi$ (mas / year)	$\mu_\alpha \pm \sigma_\alpha$ (mas/year)	$\mu_\delta \pm \sigma_\delta$	Ref.
J0034-0721	0.93 ± 0.08	10.37 ± 0.08	-11.13 ± 0.16	7
J0055+5117	0.349 ± 0.055	10.49 ± 0.085	-17.352 ± 0.204	1
J0102+6537	0.399 ± 0.045	9.252 ± 0.081	1.828 ± 0.206	1
J0108+6608	0.468 ± 0.035	-32.754 ± 0.036	35.162 ± 0.051	1
J0139+5814	0.37 ± 0.04	-19.11 ± 0.07	-16.6 ± 0.07	7
J0147+5922	0.495 ± 0.093	-6.38 ± 0.101	3.826 ± 0.097	1
J0157+6212	0.554 ± 0.039	1.521 ± 0.105	44.811 ± 0.048	1
J0323+3944	1.051 ± 0.04	26.484 ± 0.059	-30.78 ± 0.029	1
J0332+5434	0.595 ± 0.025	16.969 ± 0.029	-10.379 ± 0.058	1
J0358+5413	0.91 ± 0.16	9.2 ± 0.18	8.17 ± 0.39	5
J0454+5543	0.84 ± 0.05	53.34 ± 0.06	-17.56 ± 0.14	7
J0601-0527	0.478 ± 0.045	-7.348 ± 0.077	-15.227 ± 0.105	1
J0614+2229	0.282 ± 0.031	-0.233 ± 0.053	-1.224 ± 0.065	1
J0629+2415	0.333 ± 0.054	3.629 ± 0.193	-4.607 ± 0.153	1
J0630-2834	3.009 ± 0.409	-46.3 ± 0.99	21.26 ± 0.52	6
J0659+1414	3.47 ± 0.36	44.07 ± 0.63	-2.4 ± 0.29	8
J0729-1836	0.489 ± 0.098	-13.072 ± 0.125	13.252 ± 0.456	1
J0814+7429	2.31 ± 0.04	24.02 ± 0.09	-43.96 ± 0.35	2
J0820-1350	0.51 ± 0.04	21.64 ± 0.09	-39.44 ± 0.05	7
J0826+2637	2.01 ± 0.013	62.994 ± 0.021	-96.733 ± 0.085	1
J0922+0638	0.83 ± 0.13	18.8 ± 0.9	86.4 ± 0.7	4,9
J0953+0755	3.82 ± 0.07	-2.09 ± 0.08	29.46 ± 0.07	2
J1136+1551	2.687 ± 0.018	-73.785 ± 0.031	366.569 ± 0.072	1
J1239+2453	1.16 ± 0.08	-106.82 ± 0.17	49.92 ± 0.18	2
J1321+8323	0.968 ± 0.14	-52.674 ± 0.099	32.373 ± 0.204	1
J1509+5531	0.47 ± 0.03	-73.64 ± 0.05	-62.65 ± 0.09	7
J1532+2745	0.624 ± 0.096	1.542 ± 0.127	18.932 ± 0.118	1
J1543+0929	0.13 ± 0.02	-7.61 ± 0.06	-2.87 ± 0.07	7
J1559-4438	0.384 ± 0.081	1.52 ± 0.14	13.15 ± 0.05	6
J1607-0032	0.91 ± 0.046	-26.501 ± 0.066	27.082 ± 0.451	1
J1623-0908	0.586 ± 0.101	-10.769 ± 0.131	23.509 ± 0.166	1
J1645-0317	0.252 ± 0.028	-1.011 ± 0.051	20.523 ± 0.205	1
J1703-1846	0.348 ± 0.049	-0.751 ± 0.102	16.962 ± 0.23	1
J1754+5201	0.16 ± 0.029	-3.95 ± 0.047	1.101 ± 0.072	1
J1820-0427	0.351 ± 0.055	-7.318 ± 0.074	15.883 ± 0.088	1
J1833-0338	0.408 ± 0.067	-17.409 ± 0.158	15.038 ± 0.337	1
J1840+5640	0.657 ± 0.065	-31.212 ± 0.033	-29.079 ± 0.082	1
J1901-0906	0.51 ± 0.067	-7.531 ± 0.045	-18.211 ± 0.159	1
J1913+1400	0.185 ± 0.027	-5.265 ± 0.072	-8.927 ± 0.065	1
J1932+1059	2.78 ± 0.06	94.06 ± 0.09	43.24 ± 0.17	3
J1937+2544	0.318 ± 0.031	-10.049 ± 0.042	-13.055 ± 0.039	1
J2006-0807	0.424 ± 0.101	-6.176 ± 0.07	-10.616 ± 0.174	1
J2018+2839	1.03 ± 0.1	-2.64 ± 0.21	-6.17 ± 0.38	2
J2022+2854	0.61 ± 0.08	-3.46 ± 0.17	-23.73 ± 0.21	3
J2022+5154	0.78 ± 0.07	-5.03 ± 0.27	10.96 ± 0.17	3
J2048-1616	1.05 ± 0.03	113.16 ± 0.02	-4.6 ± 0.28	7
J2055+3630	0.17 ± 0.03	1.04 ± 0.04	-2.46 ± 0.13	7
J2113+2754	0.704 ± 0.023	-27.981 ± 0.052	-54.432 ± 0.096	1
J2113+4644	0.454 ± 0.077	9.525 ± 0.148	8.846 ± 0.09	1
J2144-3933	6.051 ± 0.56	-57.89 ± 0.88	-155.9 ± 0.54	6
J2149+6329	0.356 ± 0.072	15.786 ± 0.131	11.255 ± 0.284	1
J2157+4017	0.28 ± 0.06	16.13 ± 0.1	4.12 ± 0.12	7
J2225+6535	1.203 ± 0.204	147.22 ± 0.243	126.532 ± 0.115	1
J2305+3100	0.223 ± 0.033	-3.737 ± 0.082	-15.571 ± 0.163	1
J2313+4253	0.93 ± 0.07	24.15 ± 0.1	5.95 ± 0.13	7
J2346-0609	0.275 ± 0.036	37.39 ± 0.042	-20.23 ± 0.107	1
J2354+6155	0.412 ± 0.043	22.755 ± 0.056	4.888 ± 0.033	1

Table D1. List of normal radio pulsars used in the search. 1 – Deller et al. (2018), 2 – Brisken et al. (2002), 3 – Kirsten et al. (2015), 4 – Chatterjee et al. (2001), 5 – Chatterjee et al. (2004), 6 – Deller et al. (2009), 7 – Chatterjee et al. (2009), 8 – Brisken et al. (2003b), 9 – Brisken et al. (2003a)

PSR name	$\varpi \pm \sigma_\varpi$ (mas / year)	$\mu_\alpha \pm \sigma_\alpha$ (mas/year)	$\mu_\delta \pm \sigma_\delta$	Ref.
J0437-4715	6.396 ± 0.054	121.679 ± 0.052	-71.82 ± 0.086	1
J0613-0200	0.9 ± 0.2	1.85 ± 0.02	-10.35 ± 0.04	2
J0751+1807	0.82 ± 0.17	-2.73 ± 0.05	-13.4 ± 0.3	3
J1012+5307	0.71 ± 0.17	2.609 ± 0.008	-25.482 ± 0.011	3
J1022+1001	1.387 ± 0.041	-14.921 ± 0.05	5.611 ± 0.035	4
J1023+0038	0.731 ± 0.022	4.76 ± 0.03	-17.34 ± 0.04	5
J1300+1240	1.41 ± 0.08	46.44 ± 0.08	-84.87 ± 0.32	6
J1455-3330	0.99 ± 0.22	7.88 ± 0.05	-1.9 ± 0.12	7
J1600-3053	0.5 ± 0.07	-0.98 ± 0.02	-7.1 ± 0.06	2
J1614-2230	1.5 ± 0.1	3.8 ± 0.01	-32.5 ± 0.7	2
J1643-1224	1.27 ± 0.19	5.94 ± 0.05	3.94 ± 0.18	8
J1713+0747	0.95 ± 0.06	4.75 ± 0.17	-3.67 ± 0.16	9
J1738+0333	0.68 ± 0.05	7.037 ± 0.005	5.073 ± 0.012	10
J1741+1351	0.6 ± 0.1	-8.98 ± 0.02	-7.42 ± 0.02	2
J1744-1134	2.3 ± 0.1	18.8 ± 0.01	-9.29 ± 0.06	2
J1909-3744	0.92 ± 0.03	-9.516 ± 0.004	-35.77 ± 0.01	2
J1918-0642	0.9 ± 0.1	-7.15 ± 0.02	-5.97 ± 0.05	2
J2043+1711	0.64 ± 0.08	-5.72 ± 0.01	-10.84 ± 0.02	2
J2124-3358	2.4 ± 0.4	-14.14 ± 0.04	-50.08 ± 0.09	8
J2145-0750	1.603 ± 0.063	-9.491 ± 0.052	-9.114 ± 0.09	4
J2222-0137	3.743 ± 0.01	44.72 ± 0.02	-5.64 ± 0.06	11

Table E1. List of MSPs used in the search. 1 – Deller et al. (2008), 2 – Arzoumanian et al. (2018), 3 – Desvignes et al. (2016), 4 – Deller et al. (2018), 5 – Deller et al. (2012), 6 – Yan et al. (2013), 7 – Guillemot et al. (2016), 8 – Reardon et al. (2016), 9 – Chatterjee et al. (2009), 10 – Freire et al. (2012), 11 – Deller et al. (2013),

MSP	Gaia counterpart Gaia DR2 ID	g (mag)	$\varpi \pm \sigma_\varpi$ (mag)	$\mu_\alpha \pm \sigma_\alpha$ (mas / year)	$\mu_\delta \pm \sigma_\delta$ (mas/year)
J0437-4715	4789864076732331648	20.41	8.325 ± 0.678	122.864 ± 1.197	-71.166 ± 1.67
J1012+5307	851610861391010944	19.63	1.326 ± 0.414	2.977 ± 0.526	-26.944 ± 0.632
J1023+0038	3831382647922429952	16.27	0.728 ± 0.143	4.751 ± 0.135	-17.348 ± 0.135
J1024-0719	3775277872387310208	19.18	0.529 ± 0.426	-35.519 ± 0.64	-47.932 ± 0.659
J1843-1113	4106823440438736384	19.8	0.787 ± 0.643	-3.241 ± 1.83	-7.274 ± 2.171

Table E2. Identified optical counterparts to millisecond radio pulsars.

explosion which imparts the natal kick. The common envelope evolution is modelled through so called α -prescription (Paczynski 1976; de Kool et al. 1987; Livio & Soker 1988; de Kool 1990) with $\alpha\lambda = 2$ (model 2) The systems which went through common envelope after formation of neutron star are not interesting for us, because these are systems with extremely short orbital periods. The binaries which went through an episode of the common envelope evolution before the primary supernova explosion might have different orbital separation depending on parameters chosen for the common envelope. Therefore we decide to vary this parameter too, in our alternative model we choose $\alpha\lambda = 0.5$ (model 05). For each model we compute a sample starting from 5 million initial binaries.

Using the results of the evolution we select only bound detached systems where only one of stars is a neutron star at the end of evolution. We also checked the mass of the secondary and choose only systems where secondary is more massive than $0.5M_\odot$. The results of our simulations are presented in Table F1.

The largest apastron distance which we were able to find is 2.9×10^4 a.u for A2 model. A fraction of systems with large apastron distances is $\approx 10^{-4}$ of all NS population.

Model	max A_a a.u.	Fraction of $A_a > 10^3$ a.u.
A2	2.9×10^4	9×10^{-5}
A05	1.1×10^4	9×10^{-5}
B05	4.2×10^3	2×10^{-5}
B2	2.3×10^4	6×10^{-6}

Table F1. Results of the binary stellar population synthesis. max A_a is the largest apastron distance found in the sample. Fraction $A_a > 10^3$ a.u. is the fraction of bound systems with an NS and secondary star with mass more than $0.5M_\odot$ relative to number of all formed neutron stars.

This paper has been typeset from a $\text{\TeX}/\text{\LaTeX}$ file prepared by the author.